Simulation of the effects of chain architecture on the sorption of ethylene in polyethylene

Brian J. Banaszak, Roland Faller,[a] and Juan J. de Pablo[b]
Department of Chemical and Biological Engineering, University of Wisconsin-Madison, Madison, Wisconsin 53706

(Received 18 December 2003; accepted 25 March 2004)

An osmotic ensemble hyperparallel tempering technique has been developed to study the solubility of ethylene in amorphous linear low-density polyethylene of different chain architectures. The NERD united-atom force field (Nath, Escobedo, and de Pablo revised united-atom force field) [Nath *et al.*, J. Chem. Phys. **108**, 9905 (1998); Mol. Phys. **98**, 231 (2000); J. Chem. Phys. **114**, 3612 (2001)] is used in all simulations. We have investigated the effect of polyethylene chain length and branching on ethylene solubility. In this study, we have considered short-chain branching of amorphous linear low-density ethylene-1-hexene copolymers under typical polymerization reactor conditions. It is observed that, in the polymer, ethylene prefers to reside in the vicinity of polymer chain ends. This clustering causes a decrease in ethylene solubility with polymer chain length. When short-chain branches are introduced to a linear polymer chain, however, the chain-end clustering effect is counteracted by a higher density, thereby leading to an ethylene solubility almost identical to that in the linear polymer. © *2004 American Institute of Physics.* [DOI: 10.1063/1.1751178]

I. INTRODUCTION

In the commercial gas-phase manufacturing of linear low-density polyethylene (PE), a higher α-olefin, typically 1-butene, 1-hexene, or 1-octene, is used as a comonomer. In order to develop a sound understanding of the kinetics of the polymerization process, and hence the quality of the product resin, precise knowledge of the solubility of monomers or other small molecule solutes in PE is required under reaction conditions. Recent evidence suggests that, in reaction mixtures of small molecule solutes (methane, ethylene, 1-hexene, and nitrogen) and linear amorphous PE, the solutes exhibit a tendency to cluster near chain ends.[1,2] It is therefore reasonable to anticipate that polyolefin chain length and branching could have a pronounced effect on monomer sorption. To evaluate the merit of this hypothesis, we have developed an osmotic ensemble hyperparallel tempering technique that permits simulation of the solubility of monomers and comonomers in polyolefins of arbitrary chain architecture. The osmotic ensemble was developed due to difficulties we encountered with implementing parallel tempering techniques[3,4] within the Gibbs ensemble[5–8] framework. It provides a means of eliminating the need to simulate a second gas phase in a Gibbs ensemble when one of the components does not exist (or is negligible) in that phase. The ensemble is similar to the grand canonical ensemble[9] and the SPECS (simulation of phase equilibria of long chain systems) method introduced by Theodorou and co-workers,[10] as it is a single-simulation-cell ensemble used to study phase equilibria. In the osmotic ensemble considered here, a polymer-rich phase constrained to be in equilibrium with another phase is simulated; it is assumed that no polymer exists in that other phase. In the ensemble, the number of polymer molecules, pressure, temperature, and the absorbing species' chemical potentials are specified. In contrast to the grand canonical ensemble, it is possible to specify the pressure and to allow the simulation cell volume to fluctuate. We use the term ''osmotic ensemble hyperparallel tempering'' to denote this ensemble when it is used in combination with parallel tempering techniques.[3,4]

In addition, hybrid molecular dynamics/Monte-Carlo (MC) schemes have been devised for both molecule displacement moves at constant volume and pressure, thereby accelerating greatly the performance of our computational algorithms. These techniques are considerably faster than a standard Gibbs ensemble formalism, and have allowed us to conduct a systematic study of short-chain branching on the thermodynamic properties of ethylene/polyolefin mixtures. In this study, we consider amorphous linear low-density ethylene-1-hexene copolymers under typical reactor conditions. We examine two different branching structures. The number of branches per 100 backbone repeat units is 20 in all cases; each branch is four carbons long. In addition, we have verified the technique with infinite dilution calculations and have devised a method to extrapolate partial molar volume data from osmotic ensemble results.

The article is organized as follows: In Sec. II, we present the ethylene and polyethylene molecular models implemented in this work. In Sec. III, we describe the proposed osmotic ensemble hyperparallel tempering technique and provide a brief overview of the infinite dilution method for calculating gas sorption in polyethylene. The full details of the specific simulations conducted in this work are also included in this section. Section IV describes how to extrapolate partial molar volumes from osmotic ensemble results. In

[a]Current address: Department of Chemical Engineering and Materials Science, University of California Davis, Davis, CA 95616.
[b]Author to whom correspondence should be addressed. Electronic mail: depablo@engr.wisc.edu

Sections V A and V B, we present results for ethylene sorption in PE of different architectures. In Section V C we analyze site–site intermolecular radial distribution functions. We conclude in Sec. VI with a few remarks concerning the solubility of small molecules in polymers and the possibilities of molecular simulations in regard to the study of realistic mixtures of industrial interest.

II. MOLECULAR MODELS

All simulations employ the Nath, Escobedo, and de Pablo revised (NERD) force field,[1,11–13] in which united-atom sites represent CH_n groups in ethylene and polymer chain molecules. The force-field parameters can be found in the original references. A Lennard-Jones potential energy function is adopted for nonbonded interactions. This includes site–site interactions for sites on the same molecule located more than three bonds apart and sites located on different molecules. A torsional potential energy function is imposed on rotations about carbon–carbon bonds.[14] Bond stretching and bond-angle bending are controlled by means of a harmonic potential. For nonbonded, unlike pair interactions, Lorentz–Berthelot combining rules are used, which in previous work have been shown to be suitable for alkane mixtures.[15] In all calculations, a cutoff radius of 10.0 Å is employed for Lennard-Jones interactions, and standard tail corrections[9,16] are implemented. The NERD force field has been shown to provide good agreement with experimental phase-equilibria data for pure alkanes and alkenes, and their binary and ternary mixtures.[1,11–13,15]

Polyethylene chains of 35, 49, 100, and 500 ethylene monomers (70, 98, 200, and 1000 carbons) are considered to examine the effect of polymer chain length on ethylene solubility. Commercial linear low-density PE has short-chain branches introduced by the addition of a comonomer. We therefore investigate controlled ethylene-1-hexene polymers in this work; namely polyethylene molecules with 20 mole % 1-hexene and 80 mole % ethylene. Backbones of 35 monomers (98 carbons) are examined, and two types of 1-hexene distributions are considered. The first type contains a repetitive pattern of four ethylenes followed by one 1-hexene (designated type 1 branched C_{98}). The second type contains a repetitive pattern of eight ethylenes followed by two 1-hexenes (designated type 2 branched C_{98}), so as to have the same density of 1-hexenes as in the first case. In all cases, the stereochemistry of the short branches is random. To illustrate the difference between type 1 and type 2 branched structures, Fig. 1 shows snapshots and drawings of the linear and two branched chain types with 35-monomer backbones.

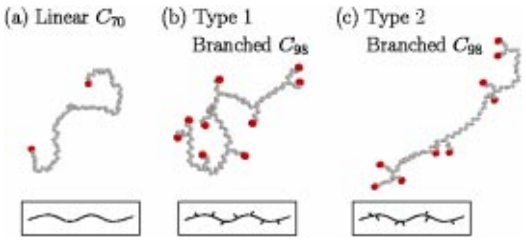

FIG. 1. Snapshots of various chains with 35 carbon backbones. The end sites are indicated in black. The insets are drawings of the structures used to illustrate the branching structures. (a) Structure for a linear C_{70} chain, (b) structure for a type 1 branched C_{98} chain, and (c) structure for a type 2 branched C_{98} chain.

III. SIMULATION METHODS

A. Osmotic ensemble

In an n-component osmotic $(\mu_1,\ldots,\mu_k,N_{k+1},\ldots,N_n,p,T)$ ensemble, the temperature (T), pressure (p), and chemical potential for $k<n$ components $(\mu_1,\ldots,\mu_k)$ are specified, while the number of molecules for $n-k$ components $(N_{k+1},\ldots,N_n)$ are held constant. The probability of the ensemble being at a given configuration $\mathbf{q}$, with N_1 molecules of type 1, N_2 molecules of type 2,..., N_k molecules of type k, and volume V is given by

$$P(\mathbf{q},V,N_1,N_2,\ldots,N_k)\propto \frac{V^{N_T}}{N_1!N_2!,\ldots,N_n!}\exp\left(-\beta U(\mathbf{q})-\beta pV+\sum_{i=1}^{k}\beta z_i N_i\right), \tag{1}$$

where p, β, z_1, $z_2,\ldots,z_k$, N_{k+1}, $N_{k+2},\ldots,N_n$ are kept constant in the osmotic ensemble and N_T is defined as the total number of molecules in the ensemble. In Eq. (1), the reduced chemical potential of component i (βz_i) is defined as

$$\beta z_i=\ln[\lambda_i^{-3}e^{\beta\mu_i}]. \tag{2}$$

The results of two-component solute i /polyethylene osmotic $(\mu_i N_{\mathrm{PE}} pT)$ ensemble simulations are compared to those of solubility calculations for solute i in PE at infinite dilution using a test-molecule insertion method.[9,17] In this method, an $N_{\mathrm{PE}}pT$ simulation is conducted and test insertions of solute i are conducted. It can be shown that the weight-average Henry's constant of solute i (H_i) in PE is

$$H_i=\left(\frac{MW_{\mathrm{PE}}}{MW_i}\right)\frac{\rho_{\mathrm{PE}}}{\beta}\frac{\langle V\rangle_{N_{\mathrm{PE}}pT}}{\langle VW^{\mathrm{ext}}_{\mathrm{test}\ i}\rangle_{N_{\mathrm{PE}}pT}}, \tag{3}$$

where MW_{PE} is the molecular weight of PE, MW_i is the molecular weight of solute i, and $W^{\mathrm{ext}}_{\mathrm{test}\,i}$ is the Rosenbluth weight[18] for the test-particle insertion of solute i (additional details on the Rosenbluth weight are provided in Sec. III B). Equation (3) assumes that molecule i does not include intramolecular nonbonded interactions (i.e., only bond stretching, bond bending, and torsional interactions are present), as is the case for ethylene. Assuming infinitely dilute conditions and an ideal gas phase for the solute, the solubility of i is equal to p/H_i. More details on this technique are provided in Appendix A.

B. Monte-Carlo moves

Three types of moves are used in the osmotic ensemble simulations to sample $\mathbf{q}$, V, $N_1,\ldots,N_k$ with probabilities dictated by Eq. (1); these consist of particle displacement moves at constant volume, particle displacement moves with chang-

ing volume, and particle insertion and deletion moves for the first $k<n$ components. For each move, the acceptance probability is given by

$$P_{\text{accept}}=\min\left[1,\frac{\alpha(\text{tr}\rightarrow o)P_{\text{tr}}}{\alpha(o\rightarrow\text{tr})P_o}\right], \tag{4}$$

where o denotes the system configuration before the move, tr denotes the trial configuration, P_i is the probability of being in configuration i as given in Eq. (1), and $\alpha(i\rightarrow j)$ is the transition probability of proposing a move from state i to state j.

Constant volume molecule displacements are conducted by means of a constant volume hybrid Monte-Carlo (CVHMC) procedure.[19,20] In the CVHMC procedure, a specified number of molecular dynamics (MD) steps (with a specified time step per MD step) are used to generate a global trial MC move. Using Eq. (4), the acceptance probability for such moves is given by

$$P_{\text{accept,CVHMC}}=\min[1,e^{-\beta(\Delta U_{o\rightarrow\text{tr}}+\Delta K_{o\rightarrow\text{tr}})}], \tag{5}$$

where $\Delta K_{o\rightarrow\text{tr}}$ is the change in kinetic energy from the old to the new trial state.

Volume displacements are conducted by means of a constant-pressure hybrid Monte-Carlo (CPHMC) procedure.[21,22] In the CPHMC procedure, a specified number of reversible Berendsen molecular dynamics[23,24] steps (with a specified time step per MD step) are used to generate a global trial MC move. Using Eq. (4), the acceptance probability for such moves is given by

$$P_{\text{accept,CPHMC}}=\min\left[1,\left(\frac{V_{\text{tr}}}{V_o}\right)^{N_{\text{site}}}e^{-\beta(\Delta U_{o\rightarrow\text{tr}}+p\Delta V_{o\rightarrow\text{tr}}+\Delta K_{o\rightarrow\text{tr}})}\right], \tag{6}$$

where p is the specified pressure and N_{site} is the total number of sites in the simulation.

In the osmotic ensemble used in this study, no PE chains are inserted into or deleted from the simulation cell. Insertion and deletion moves for ethylene are conducted by means of configurational bias (CB) moves[25–27] at constant volume. Trial orientations within the CB technique are generated via an acceptance–rejection scheme.[9,28] In this scheme, the first site of a molecule is inserted at a random position within the simulation cell. For other sites in a molecule, a position with a random direction on a sphere[29] and a bond length distributed according to a harmonic spring[9] is generated. A trial position is selected according to the probability of the new bonded interactions introduced with the site (bond stretching, bond bending, and torsional interactions).[28] The acceptance criteria for inserting one molecule of type i are given by

$$P_{\text{accept,CB-ins}}=\min\left[1,W_i^{\text{ext}}\frac{V}{N_i+1}C_{\text{chn }i}e^{\beta z_i}\right], \tag{7}$$

where W_i^{ext}, the Rosenbluth weight of molecule i associated with the growth or deletion process, is given by

$$W_i^{\text{ext}}=\prod_{j=1}^{n_i}N_{\text{samp}}^{-1}(j)\sum_{k=1}^{N_{\text{samp}}(j)}e^{-\beta U_k^{\text{nonbonded}}(j)}. \tag{8}$$

In Eq. (8), n_i is the number of sites for a type i molecule, $N_{\text{samp}}(j)$ is the number of trial insertions of site j in the growing or deleted molecule, and $U_k^{\text{nonbonded}}(j)$ is the nonbonded potential energy due to the k trial site of site j in the type i molecule. In Eq. (7), $C_{\text{chn }i}$ is $\Pi_{j=1}^{n}C_{\text{chn }i,\text{site }j}$, where $C_{\text{chn }i,\text{site }j}$ is given by

$$C_{\text{chn }i,\text{site }j}=\int d\mathbf{r}e^{-\beta U_{\text{chn }i,\text{site }j}^{\text{bonded}}(\mathbf{r})}. \tag{9}$$

By defining βz_i^{mod} as $\beta\mu_i-\ln\lambda_i^3+\ln C_{\text{chn }i}$, or equivalently $\beta z_i+\ln C_{\text{chn }i}$, the acceptance probability for inserting one molecule of type i can be rewritten as

$$P_{\text{accept,CB-ins}}=\min\left[1,W_i^{\text{ext}}\frac{V}{N_i+1}e^{\beta z_i^{\text{mod}}}\right]. \tag{10}$$

The acceptance probability for deleting one molecule of type i is obtained in an analogous fashion and is given by

$$P_{\text{accept,CB-del}}=\min\left[1,\frac{1}{W_i^{\text{ext}}}\frac{N_i}{V}e^{-\beta z_i^{\text{mod}}}\right]. \tag{11}$$

Additional constant-volume molecular displacement moves considered in a few simulations in this work include CB inner-chain rebridging,[30] end-chain CB, and CB reptation moves. These moves are similar to the CB insertion/deletion moves, and further information can be found in the original references.[25–27,30] In order to characterize pure PE and to perform infinite dilution calculations, $N_{\text{PE}}pT$ ensemble simulations have also been conducted in this work. With the exception of ethylene insertion and deletion moves, the same type of MC moves are used in the $N_{\text{PE}}pT$ simulations as with the osmotic ensemble simulations.

C. Parallel tempering in an osmotic ensemble

The osmotic ensemble described in subsection B is implemented in the context of a parallel tempering (PT) technique.[3,4] Yan *et al.* studied Lennard-Jones atoms and polymeric systems in a grand-canonical formalism[4,31] and found significant speedup with the PT scheme.

In this technique, N osmotic replicas are run independently using regular osmotic ensemble moves. Attempts are also made to exchange the extensive variables of two replicas with acceptance related to their partition functions. For an n-component osmotic ensemble with $k<n$ components at constant chemical potentials, and $n-k>0$ components at constant number of molecules, each replica may be at different temperature, pressure, and chemical potential for the k components. However, the same extensive variables are kept constant in each replica (the number of molecules for $n-k$ components is the same and constant for each replica in the osmotic ensemble formalism). For randomly chosen pairs, an exchange between replica configurations $\mathbf{x_l}$ and $\mathbf{x_m}$ is accepted according to

$$P_{\text{accept}}(\mathbf{x_l}\leftrightarrow\mathbf{x_m})=\min\left[1,\frac{P_{\text{osmotic},l}(\mathbf{x_m})P_{\text{osmotic},m}(\mathbf{x_l})}{P_{\text{osmotic},l}(\mathbf{x_l})P_{\text{osmotic},m}(\mathbf{x_m})}\right], \tag{12}$$

where $P_{\text{osmotic},i}(\mathbf{x_j})$ is the probability of replica i having configuration $\mathbf{x_j}$. Inserting Eq. (1) into (12) yields the following acceptance criteria for swapping osmotic ensemble replica configurations:

$$P_{\text{accept}}(\mathbf{x_l}\leftrightarrow\mathbf{x_m}) = \min\Bigg[1, \exp\Bigg(-\beta_l \Delta U_l - \beta_l p_l \Delta V_l + \sum_{i=1}^{k} \beta_l z_{i,l}^{\text{mod}} \Delta N_{i,l}\Bigg) \times \exp\Bigg(-\beta_m \Delta U_m - \beta_m p_m \Delta V_m + \sum_{i=1}^{k} \beta_m z_{i,m}^{\text{mod}} \Delta N_{i,m}\Bigg)\Bigg], \tag{13}$$

where

$$\Delta A_m = -\Delta A_l = A(\mathbf{x_m}) - A(\mathbf{x_l}), \tag{14}$$

and where A_j is a varying configurational-dependent variable in replica j (e.g., the internal energy U_j, the replica volume V_j, or the number of molecules of type i, $N_{i,j}$).

D. Gas phase chemical potential

Gas phase chemical potentials required for osmotic ensemble simulations are calculated using a configurational bias test molecule insertion scheme within an NpT simulation.[9] The reduced chemical potential of molecule i (βz_i^{mod}) is determined by

$$z_i^{\text{mod}} = \beta\mu_i - \ln \lambda_i^3 + \ln C_{\text{chn } i} = \ln(N_i + 1) - \ln\langle VW_{\text{test } i}^{\text{ext}}\rangle \tag{15}$$

where $W_{\text{test } i}^{\text{ext}}$ is the Rosenbluth weight associated with a test molecule of type i inserted into the system.

For this study, the reduced chemical potential of pure ethylene gas is determined for various conditions. NpT simulations consist of 80% constant volume CB moves and 20% random volume moves. Each CB move is performed using ten trial orientations per site. Random volume moves are conducted with a maximum volume change of $10-100\sigma_{LJ,\min}^3$ for the various conditions considered. All simulations are run for 10^6 steps with 200 ethylenes per simulation cell; 250 test ethylene insertions are conducted every ten steps in a configurational bias manner with ten trial orientations per site. The average $VW_{\text{est ethylene}}^{\text{ext}}$ is used with Eq. (15) to find the effective ethylene chemical potential for a given set of conditions.

E. Simulation details

In this work, eight osmotic replicas are run in parallel for polyethylene chains of 200 carbons and less. Each replica has the same temperature (105 °C) and the same number of polymer molecules. Replicas differ in their pressure and their ethylene chemical potentials, with pressures ranging from 5 to 54 bar.

For PE modeled with 1000 carbons, three osmotic ensemble hyperparallel tempering cases are simulated. For each case, ten osmotic replicas are run in parallel. Replicas have the same pressure and the same number of polymer molecules. Replicas differ in their temperature and their ethylene chemical potentials, with temperatures ranging from 70 to 200 °C. The three cases are conducted for pressures of 9, 18, and 30 bar. The results at 105 °C are presented in this work.

TABLE I. Conditions for ethylene/amorphous PE osmotic ensemble simulations. All conditions are at 105 °C.

PE model	Pressure [bar]	$z_{\text{eth}}^{\text{mod}}$
C_{70}, C_{98}s, C_{200}		
	5	−9.266
	12	−8.409
	19	−7.967
	26	−7.672
	33	−7.451
	40	−7.277
	47	−7.134
	54	−7.013
C_{1000}		
	9	−8.689
	18	−8.019
	30	−7.539

Effective ethylene chemical potentials for each condition are calculated as described in subsection D. The results can be found in Table I.

Between 2 and 15 PE chains are in a simulation cell, depending on the specified PE architecture. For the shorter C_{70} and C_{98} chains, 15 PE chains are in a simulation cell. For these systems, we have found the results to be identical to those of simulations with 10 PE chains. For the PE chains of 200 carbons, 9 PE chains are in a simulation cell. The results for these systems are consistent with the trends of the shorter and longer PE chain simulations. For PE chains of 1000 carbons, two PE chains are in a simulation cell. Note that we have also studied systems of up to eight PE chains of 1000 carbons and obtained results identical to those for two PE chains. In the osmotic ensemble simulations, the number of ethylenes is in the range of 6–12 for 5 bar and 50–100 for 54 bar at 105 °C.

Details of the MC move parameters and simulation specifications for the osmotic and $N_{\text{PE}}pT$ simulations are provided in Tables II and III, respectively. The changing MC parameters and simulation specifications given in the tables are the result of optimizations developed throughout this work. In the infinite dilution simulations, 250 insertions of ethylene in C_{70} are conducted every ten MC steps. Three infinite dilution simulations with independent initial equilibrium configurations and the specifications shown in Table III have been conducted at 1 bar and 105 °C.

IV. PARTIAL MOLAR PROPERTIES

In addition to solubility predictions, osmotic ensemble simulations also provide partial molar quantities. For a two-component system, a partial molar quantity for component 1 is defined as

$$\overline{b}_1 = \left(\frac{\partial\langle B\rangle_{N_1N_2pT}}{\partial N_1}\right)_{N_2,p,T}, \tag{16}$$

TABLE II. Parameters used for MC moves. For moves with parameters different for ethylene and PE, the molecule for the parameter is specified in parentheses.

MC move	Number of sites/move[a]	Number of trial insertions/site	Number of MD steps per move	reduced MD time step[b]
CB moves				
Ethylene insertion/deletion	2	10	⋯	⋯
Test ethylene insertion[c]	2	15	⋯	⋯
End-chain	1–6 (PE) 1–2 (ethylene)	10	⋯	⋯
Reptation	1–4 (PE)	10	⋯	⋯
Inner chain rebridging	2–6 (PE)	10	⋯	⋯
Hybrid-MC moves				
CPHMC	⋯	⋯	5[d]	0.0005[e]
			15[f]	0.001[g]
CVHMC	⋯	⋯	5[d]	0.0005[e]
			15[f]	0.0018[g]

[a]Randomly chosen between given range.
[b]Reduced in terms of σ, ϵ, and the mass of Lennard-Jones site with minimum σ.
[c]Used in $N_{PE}pT$ infinite dilution simulations.
[d]For C_{70}, C_{98}, and C_{200} osmotic ensemble simulations.
[e]For C_{70} and C_{98} osmotic ensemble simulations.
[f]For $N_{PE}pT$, C_{200} osmotic ensemble, and C_{1000} osmotic ensemble simulations.
[g]For $N_{PE}pT$ and C_{1000} osmotic ensemble simulations.

where $\langle B\rangle_{N_1N_2pT}$ is any relevant extensive property at the specified N_1, N_2, p, and T. Note that the μ_1N_2pT osmotic ensemble is a collection of N_1N_2pT ensembles at various N_1 sampled with probabilities proportional to $e^{\beta N_1\mu_1}$. With this in mind, from an osmotic ensemble simulation, average properties at various N_1 and constant N_2, p, and T can be calculated. From Eq. (16), the partial molar quantity, $\bar{b}_1$ can be determined from the slope of a N_1 versus $\langle B\rangle_{N_1N_2pT}$ curve. After determining $\bar{b}_1$, $\bar{b}_2$ can be calculated by solving for $\bar{b}_2$ in the following thermodynamic relationship:

$$\langle B\rangle_{\mu_1N_1pT}=\langle N_1\rangle\bar{b}_1+N_2\bar{b}_2, \tag{17}$$

where $\langle B\rangle_{\mu_1N_2pT}$ is the total average value of B in the osmotic ensemble simulation.

As an illustration of the calculations of partial molar volumes, Fig. 2 shows a plot of average volume versus N_{eth} determined from an ethylene(1)/linear C_{70}(2) μ_1N_2pT simulation at 105 °C and 33 bar. From the slope, the partial molar volume of ethylene is determined. The partial molar volume of PE can be calculated by applying Eq. (17).

From knowledge of partial molar volumes, it is possible to extrapolate phase equilibria data for different pressures at a specified temperature, given a reference state result. In this work, we consider the phase equilibria between gas i and

TABLE III. Simulation specifications for osmotic and $N_{PE}pT$ ensemble simulations. The polymer model for each case is shown in the left-hand column.

PE models	PT swapping %	Distribution of non-PT swapping MC moves						Number of MC steps/system [$\times10^{-6}$]
		CPHMC %	CVHMC %	ethylene CB insertion/deletion %	End-site CB %	Reptation CB %	Inner chain rebridging %	
Osmotic simulations								
Linear C_{70}	0.01	24	6	70	⋯	⋯	⋯	3.7
Linear C_{98}	0.01	24	6	70	⋯	⋯	⋯	2.0
Type 1 branched C_{98}	0.01	24	6	70	⋯	⋯	⋯	3.7
Type 2 branched C_{98}	0.01	24	6	70	⋯	⋯	⋯	2.0
Linear C_{200}	0.1	4	1	90	⋯	5	⋯	2.0
Linear C_{1000}	0.05	1	0.25	83	1.25	4.5	10	3.0
$N_{PE}pT$ simulations								
Linear C_{70}	⋯	2.5	0.5	⋯	19	35	43	5
Linear C_{98}	⋯	2.5	0.5	⋯	19	35	43	5
Linear C_{200}	⋯	1.25	0.25	⋯	19	35	44.5	10
Linear C_{1000}[a]	0.05	0.8	0.2	⋯	10	43	46	2
Linear C_{70}[b]	⋯	0.8	0.2	⋯	33	33	33	10

[a]Simulation with parallel tempering for ten $N_{PE}pT$ ensembles at 1 bar and 70–200 °C.
[b]For infinite dilution calculations.

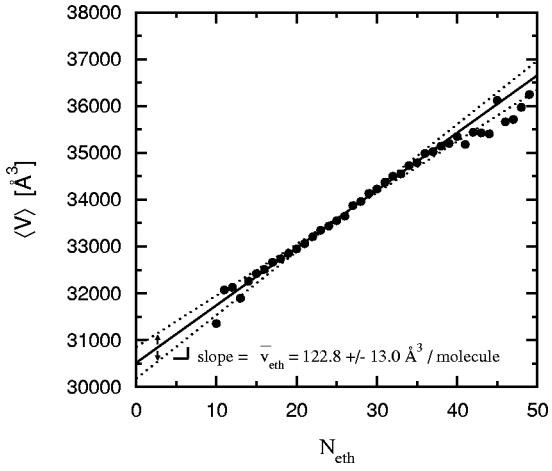

FIG. 2. Calculation of ethylene partial molar volume for ethylene/linear C_{70} mixture at 105 °C and 33 bar. The solid line is a linear fit to the simulation data and the dotted lines represent an estimated uncertainty in the fitted line.

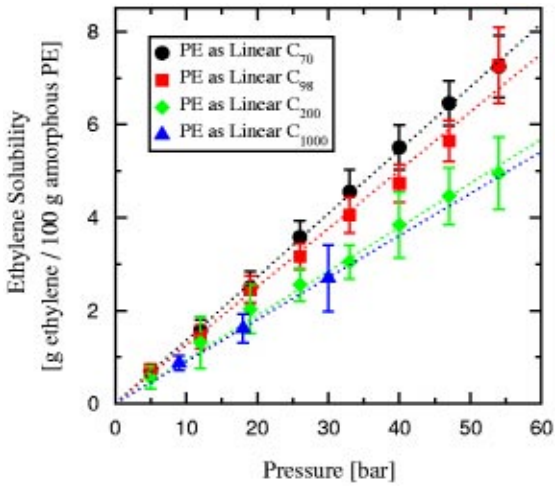

FIG. 3. Solubility of ethylene in linear PE at 105 °C as a function of pressure for various PE chain lengths. The dotted lines are linear fits to the simulation results.

solute *i*/PE mixture. By defining $\hat{f}_i^P$ as $K_i w_i$ ($\hat{f}_i^P$ is defined as the polymer phase fugacity for solute *i* in the polymer phase) and using the thermodynamic relationship for the pressure derivative of $\hat{f}_i^P$, an expression can be determined for the pressure dependence of the proportionality factor K_i at a specified temperature, as

$$K_i(T,p) = K_i^0(T,p^0)\exp\left(\frac{\overline{v_i^0}(p-p^0)}{RT}\right), \tag{18}$$

where superscript 0 indicates the reference condition, and it is assumed that $\overline{v_i}$ is insensitive to pressure. This assumption will be seen to be valid for the systems studied in this work. A more general expression for $K_i(T,p)$ can be found in Appendix C. After equating the fugacities of solute *i* in the gas and polymer phases, an expression for w_i as a function of pressure and a specified temperature is derived as

$$w_i = \frac{\varphi_i p}{K_i}, \tag{19}$$

where φ_i is the pure component fugacity coefficient for gas phase *i*.

V. RESULTS AND DISCUSSION

A. Ethylene sorption in linear polyethylene chains

Figure 3 shows the results of simulations of ethylene sorption in linear C_{70}, C_{98}, C_{200}, and C_{1000} chains. It is observed that the solubility increases linearly with increasing pressure for all chains, as expected in the Henry's law regime. In addition, there is a significant decrease in ethylene solubility when going from C_{70} to C_{1000} chains. This result confirms our original hypothesis that increasing chain length decreases ethylene solubility.[1,2] Figure 4 shows the ethylene solubility/pressure (inverse Henry's constant) versus the inverse of the chain length for various linear PE chains. As observed in Fig. 4, the ethylene solubility/pressure scales approximately linearly with the inverse of the chain length. This is consistent with previous experimental studies of carbon dioxide solubility in various linear hydrocarbons of different chain lengths.[32]

Figure 5 shows simulation results for the density of ethylene/linear amorphous PE mixtures. Simulation results for pure linear PE chains are also shown in Fig. 5. Upon extrapolating the mixture density results to pure amorphous PE, agreement with simulated pure linear PE simulations is observed. As shown in Fig. 6, the simulated pure linear PE simulations are in satisfactory agreement with the experimental data extrapolated from higher temperature results of Dee *et al.*[33] In Fig. 5, it is noted that an increase in pressure causes a decrease in the ethylene/PE mixture density. This is due to an increase in ethylene concentration in the mixture at higher pressures. It is also noted that an increase in PE chain length leads to an increase in density. This is further analyzed by studying partial molar volumes. Figure 7 shows the calculated ethylene and PE partial molar volumes for PE models of linear C_{70}-C_{200} chains. First, it is noted that the

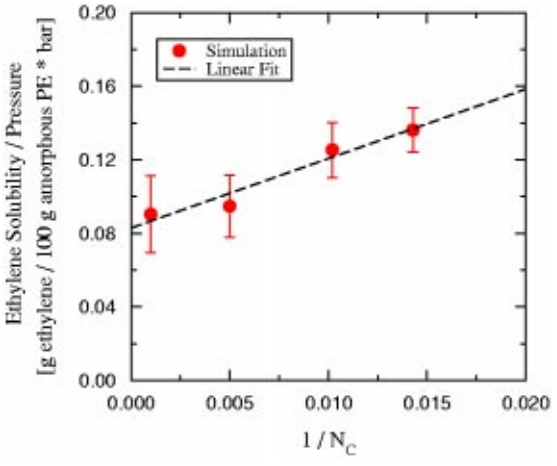

FIG. 4. Ethylene solubility/pressure for ethylene in various linear PEs at 105 °C. N_C is the number of carbons in the linear PE. The simulation error bars are estimated uncertainties based on the data in Fig. 3.

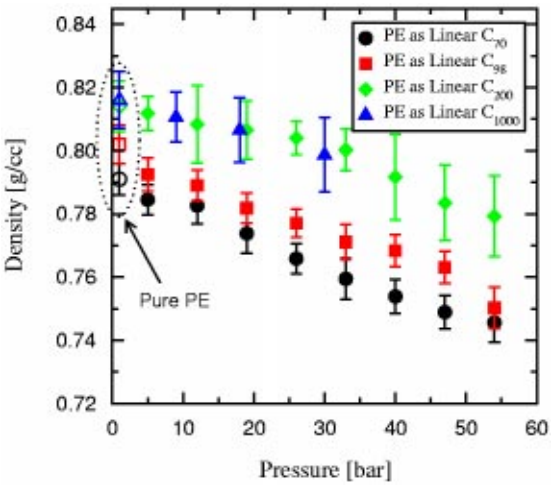

FIG. 5. Density of ethylene (eth)/linear PE mixtures at 105 °C as a function of pressure for various PE chain lengths. The closed symbols are simulated densities for the eth/PE mixtures. The open symbols are simulated densities of pure PE at 105 °C and 1 bar with shapes corresponding to the PE models indicated in the legend.

partial molar volume of ethylene is insensitive to chain length. However, the partial molar volume of PE/site appears to decrease with chain length. This explains the observed increase in density with chain length.

Figure 8 compares simulated ethylene solubility in linear C_{70} with predicted results based on the weight-average Henry's constant calculated from the infinite dilution method of Sec. III A. From the infinite dilution calculations the weight-average Henry's constant is calculated to be in the range of 755–1062 bar*(g amorphous PE/g ethylene). The corresponding upper and lower bounds for solubility predictions with this range of Henry's constant are shown in Fig. 8. The infinite dilution method yields results similar to those obtained using the osmotic ensemble technique. The infinite dilution method predicts slightly lower solubilities, which is due to the inability of this method to capture polymer swelling.

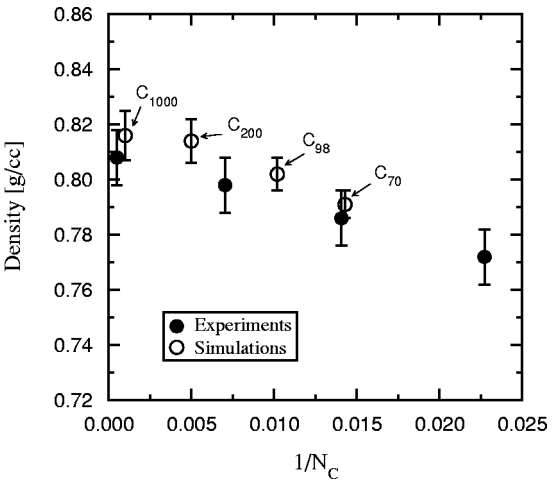

FIG. 6. Density of pure linear PE at 105 °C and 1 bar as a function of PE chain length. N_C is the number of carbons in the linear PE. The experimental densities are extrapolated from higher temperatures to 105 °C (see Ref. 33). The error bars represent the uncertainty in the extrapolation.

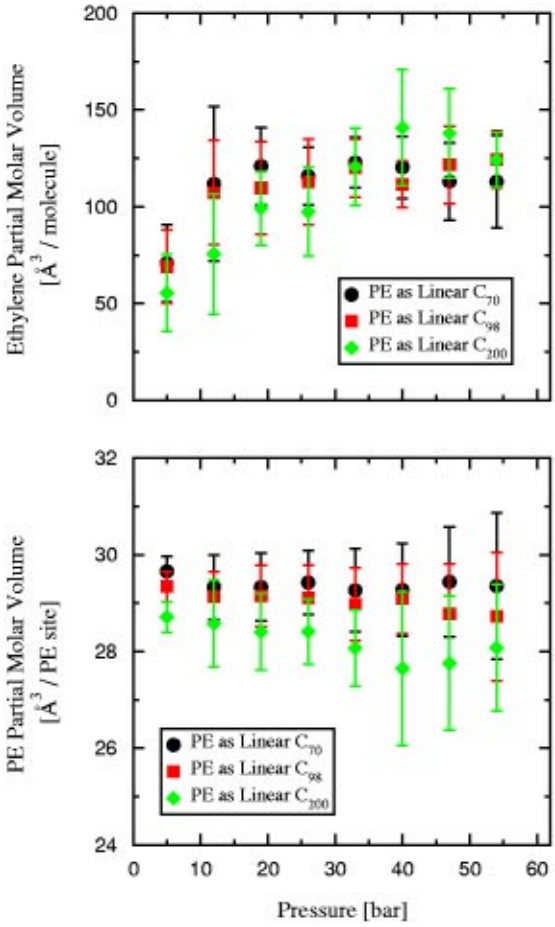

FIG. 7. Ethylene and PE site partial molar volumes for ethylene/linear PE mixtures at 105 °C as a function of pressure for various PE chain lengths. The ethylene partial molar volumes and corresponding error bars are calculated by the method described in Sec. IV and Fig. 2. The PE partial molar volumes and corresponding error bars are calculated by applying Eq. (17).

Figure 9 compares simulated ethylene solubility in linear C_{70} with predicted results based on rescaling with $\bar{v}_{eth}$ using Eqs. (18) and (19). Results are shown for ideal gas (φ_{eth} set to 1) and a nonideal gas (φ_{eth} calculated using a second-order virial equation of state) for the ethylene gas phase. The results are based on extrapolation of osmotic ensemble simulation results at 28 bar (reference state). As observed in Fig. 9, the method predicts the full simulation results accurately within the error bars of the simulation results. It should be noted that the scaling factor for K_{eth}, $\exp(\bar{v}^0_{eth}(p-p^0)/RT)$, is small for all cases, having a value between 0.93 and 1.07 for the pressures studied.

B. Ethylene sorption in ethylene-1-hexene copolymer chains

Figure 10 shows simulation predictions for ethylene sorption in linear C_{98} chains and the two types of branched C_{98} chains. Henry's law behavior is observed in all cases. From Fig. 10, it is interesting to note that ethylene solubility does not change with short-chain branching. Furthermore,

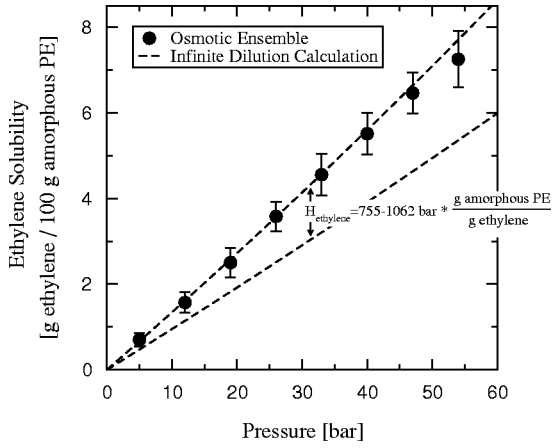

FIG. 8. Comparison of osmotic ensemble ethylene/C_{70} simulations with results based on ethylene test particle insertion into pure C_{70} at 1 bar and 105 °C. The lines represent the upper and lower bounds for solubility predictions based on the error in the Henry's law constant calculation from three independent infinite dilution simulations.

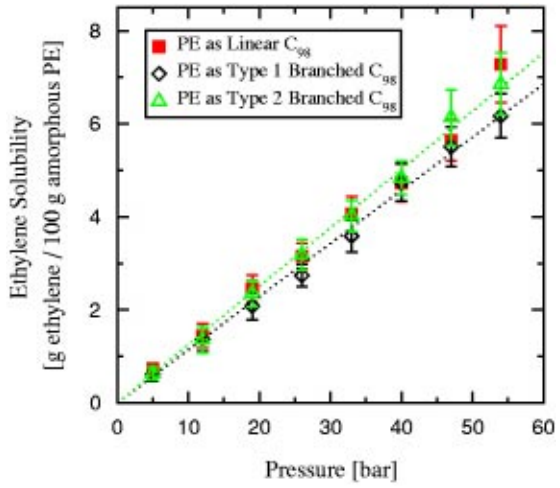

FIG. 10. Solubility of ethylene in PE at 105 °C as a function of pressure for various PE models with 98 carbons. The dotted lines are linear fits to the simulated results.

the distribution of 1-hexene along the polymer backbone does not seem to influence ethylene solubility. This is contrary to our original hypothesis that ethylene clustering near chain ends will cause an enhancement in ethylene solubility as a result of inclusion of short-chain branching.

Figure 11 shows results of simulations of polymer-phase densities for the mixtures of ethylene and PE chains of 98 carbons. It is observed that the polymer phase density increases by 2%–3% when going from systems with linear C_{98} to systems with branched C_{98}. This has profound effects on the accessible volume for molecules to sorb into the polymer phase. The free volume and clustering effects (see Sec. V C) are offset in this case, causing the solubility to be independent of branching for these PE models. This is further analyzed by studying partial molar volumes. Figure 12 shows the calculated ethylene and PE site partial molar volumes for PE models of linear and branched C_{98} chains. First, it is noted that the partial molar volume of ethylene is insensitive to branching. However, the partial molar volume of PE sites appears to decrease when branching is introduced, but appears insensitive to branching distribution. This is consistent with the increase in density with branched chains, as explained earlier.

C. Radial distribution functions

Radial distribution functions provide a means of verifying the ethylene clustering hypothesis. All radial distribution functions presented here are for simulations at 105 °C and 33 bar. Some interesting features can be seen in the ethylene site–ethylene site, PE site–PE site, and ethylene site–PE site intermolecular radial distribution functions. Figure 13 shows intermolecular site–site radial distribution functions for the ethylene/linear C_{70} mixture. Of all the radial distribution

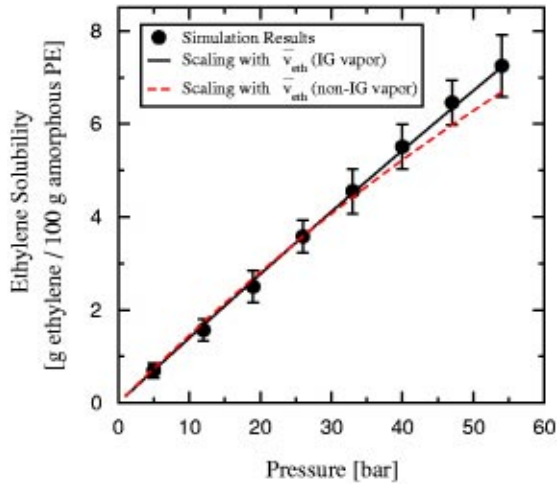

FIG. 9. Comparison of osmotic ensemble ethylene/C_{70} simulations with results based on rescaling with $\overline{v}_{eth}$ according to Eqs. (18) and (19) with the 28 bar result as the reference state. The straight line is the result based on an ideal gas assumption for the ethylene gas. The dashed line assumes a virial equation of state for the ethylene gas. All results are at 105 °C.

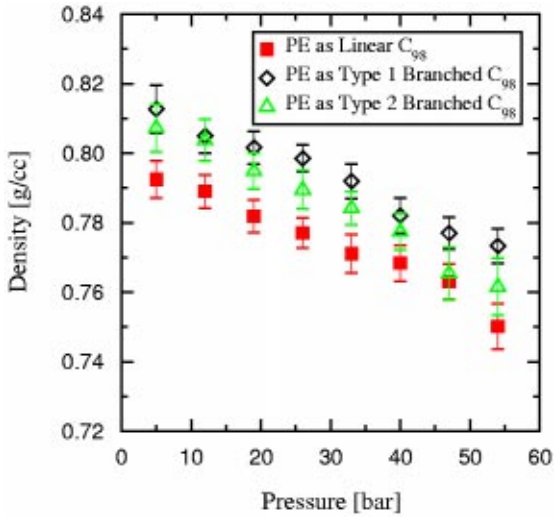

FIG. 11. Density of eth/PE mixtures at 105 °C as a function of pressure for various PE models with 98 carbons.

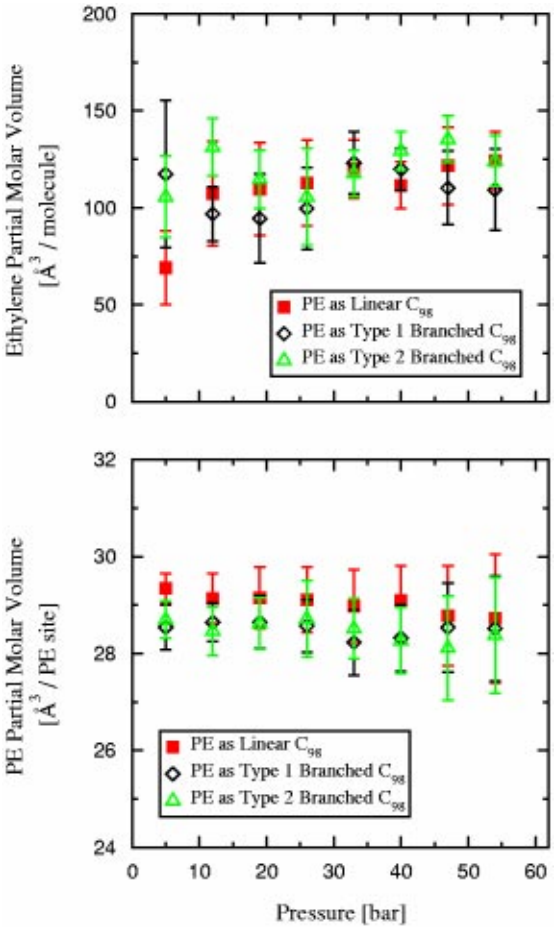

FIG. 12. Ethylene and PE site partial molar volumes for ethylene/PE mixtures at 105 °C as a function of pressure for various PE models with 98 carbons. The ethylene partial molar volumes and corresponding error bars are calculated by the method described in Sec. IV and Fig. 2. The PE partial molar volumes and corresponding error bars are calculated by applying Eq. (17).

functions in Fig. 13, the ethylene $CH_2(sp^2)$ site–ethylene $CH_2(sp^2)$ site function has the largest first peak, indicating a preference for ethylene to cluster with itself. It is interesting to note that the ethylene site–C_{70} $CH_3(sp^3)$ site (end-group site) function has a first peak at a shorter distance that is clearly larger than the ethylene site–C_{70} $CH_2(sp^3)$ site (middle site) function, and that the C_{70} end-group site–C_{70} end-group site function has a first peak at a shorter distance that is larger than the C_{70} middle-site–C_{70} middle-site function. From an entropic point of view, because the C_{70} end sites are only bonded to one other site instead of to two other sites (like the other 68, C_{70} middle sites), they will be surrounded by more available volume. Therefore, C_{70} end sites will have a tendency to ''attract'' small ethylene aggregates; hence, the ethylene site–C_{70} end-group site radial distribution function has a first peak at a shorter distance that is larger than the ethylene site–C_{70} middle-site function. This entropic effect has been observed previously.[2]

Figure 14 shows intermolecular site–site radial distribution functions for the ethylene/type 1 branched C_{98} mixture. The results are similar to those of the ethylene/C_{70} mixture. Of all the radial distribution functions in Fig. 14, the ethyl-

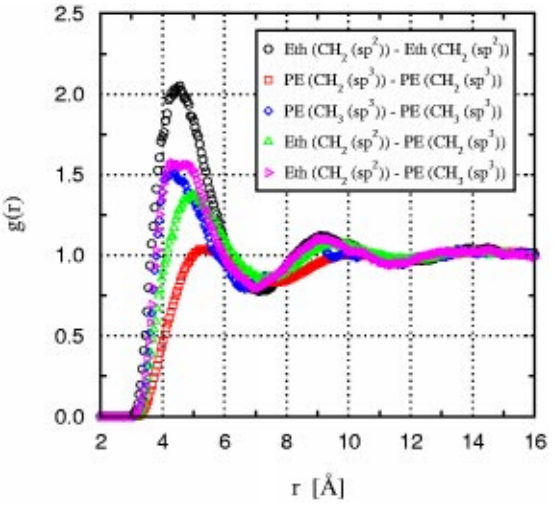

FIG. 13. Intermolecular site–site radial distribution functions in the ethylene(eth)/PE as linear C_{70} mixture at 105 °C and 33 bar.

ene site–ethylene site function has the largest first peak, indicating a preference for ethylene to cluster with itself. The ethylene site–type 1 branched C_{98} $CH_3(sp^3)$ site (end-group site) function has a first peak at a shorter distance that is clearly larger than the ethylene site–type 1 branched C_{98} $CH_2(sp^3)$ site (nonbranching middle site); this is due to the same entropic reasons as the previous case. Since the branched chains have many more end sites than the linear chains, one would expect the ethylene solubility to increase with branching for entropic reasons. However, this is not observed with the C_{98} PE models. As noted in subsection B, an offsetting density effect compensates the clustering of ethylene observed near chain ends. Figure 14 also indicates that type 1 branched C_{98} $CH(sp^3)$ sites (branching middle sites) have a tendency to suppress clustering. This is indicated by the first peak in the type 1 branched C_{98} $CH(sp^3)$ site–type 1 branched C_{98} $CH(sp^3)$ site and ethylene site–type 1 branched C_{98} $CH(sp^3)$ site functions appearing at larger dis-

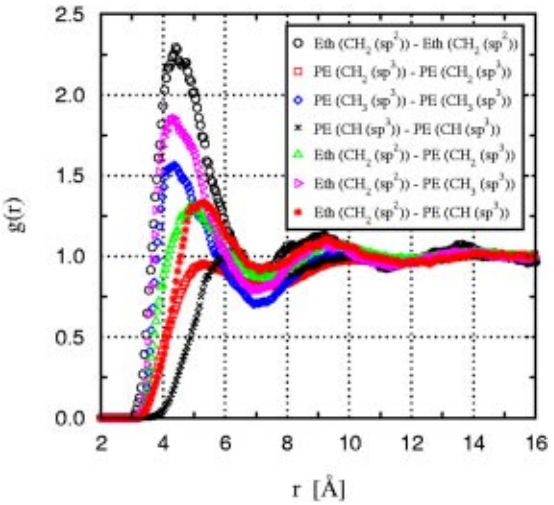

FIG. 14. Intermolecular site–site radial distribution functions in the ethylene(eth)/PE as type 1 branched C_{98} mixture at 105 °C and 33 bar.

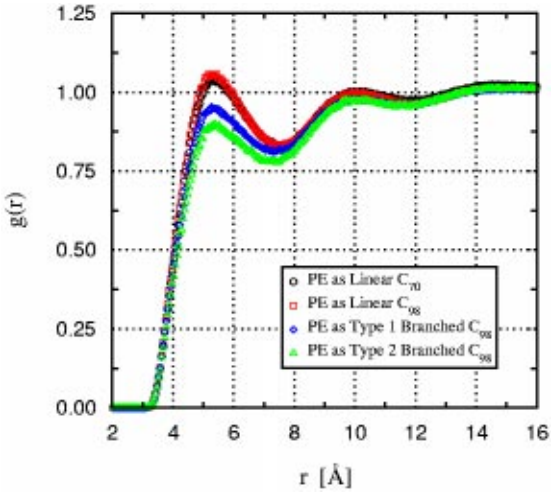

FIG. 15. Effect of branching on the intermolecular PE $CH_2(sp^3)$ site–PE $CH_2(sp^3)$ site radial distribution function in ethylene(eth)/PE mixtures at 105 °C and 33 bar.

tances as compared to the type 1 branched C_{98} $CH_2(sp^3)$ site–type 1 branched C_{98} $CH_2(sp^3)$ site and ethylene site–type 1 branched C_{98} $CH_2(sp^3)$ functions, respectively. From an entropic point of view, since the CH branching sites of type 1 branched C_{98} are bonded to three other sites, less available volume is free around these sites to attract other sites. This contributes to the observation that ethylene solubility does not increase with branching even though more chain ends are present.

Some interesting observations are noted upon comparing the radial distribution functions of linear and branched polymer models. Figure 15 shows the dependence on branching for the intermolecular PE $CH_2(sp^3)$ site–PE $CH_2(sp^3)$ site radial distribution function. It is apparent that the peak of the first coordination shell of this function decreases in magnitude with chain branching. This is due to limited free volume in the vicinity of many PE CH_2 sites near chain branches. The fact that interlocking side chains are disfavored by entropy may also play a role.

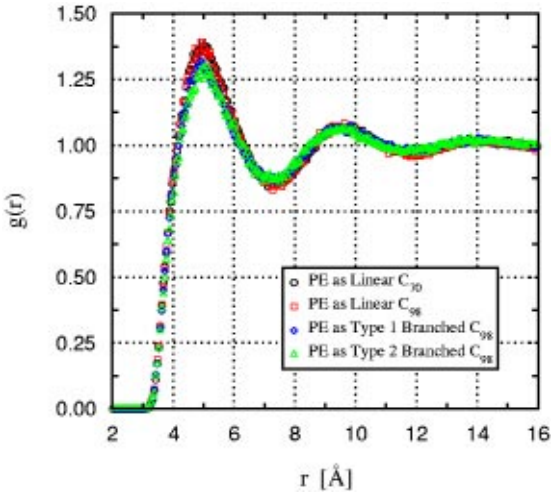

FIG. 16. Intermolecular ethylene $CH_2(sp^2)$ site–PE $CH_2(sp^3)$ site radial distribution function in ethylene(eth)/PE mixtures at 105 °C and 33 bar.

Figure 16 shows the dependence on branching for the intermolecular ethylene site–PE $CH_2(sp^3)$ site radial distribution function. It is observed that the peak of the first coordination shell of this function slightly decreases in magnitude with chain branching. Again, this is due to limited free volume near many PE CH_2 sites near chain branches.

VI. CONCLUSIONS

Monte-Carlo simulations with an osmotic ensemble hyperparallel tempering technique have been developed and conducted to study the solubility of mixtures of ethylene and polyolefins of different architectures. The NERD united-atom force field was used for this study. This force field has been tested previously for binary and ternary[1,2,11,13] mixtures of small molecules with long linear and branched alkanes, and has been shown to provide good agreement with experimental data.

Radial distribution functions for ethylene/linear PE and ethylene/branched PE mixtures have been determined. Results indicate that ethylene molecules tend to form clusters of their own in the mixture, and ethylene exhibits a tendency to reside in the vicinity of the polymer end groups. This entropic clustering has a major effect on ethylene solubility. The ethylene solubility in linear PE is seen to decrease with chain length.

Interestingly, ethylene solubility appears to be unaltered by short-chain branching. While ethylene still clusters near branch end groups, the solubility remains unaltered by the fact that the density of branched systems is slightly higher, thereby leading to an almost perfect cancellation of the clustering enhancement effect. The ethylene depletion near branching points also counteracts the entropic clustering that occurs near chain ends (which increases with chain branching). Simulations with longer side-chains would be necessary in order to elucidate this in more detail.

It is important to emphasize that the results presented for the branched architectures have random branching stereochemistry. In the amorphous phase, the stereochemistry is not expected to affect the simulation results; however, this issue should be examined in more detail in the future. Note that stereochemistry will have a major impact on the polymer crystallinity.

To predict solubilities in real, semi-crystalline polyethylene, one must take into account the elastic effect that crystalline regions have on the solubility in the amorphous regions of the material. We are currently developing a model to predict the effects of polymer crystallinity on ethylene solubilities in polyethylene. The simulation results in this work provide a good means to estimate equation of state parameters for ethylene in a hypothetical amorphous polyethylene sample at the conditions of interest. An additional parameter is then employed to characterize the crystalline structure for a specific polymeric sample.

Simulations of more architectures would prove interesting. In this work, relatively few architectures have been stud-

ied. For example, simulations of blocky polyolefin structures would be of interest in the future.

ACKNOWLEDGMENTS

The authors are grateful to Professor W. Harmon Ray at the University of Wisconsin-Madison for insightful advice throughout this project. Financial support from the U.S. Department of Energy (DE-FG02-99ER14961) is also gratefully acknowledged.

APPENDIX A: PHASE-EQUILIBRIA MODEL

A general phase-equilibria model for gas sorption in PE has been adopted throughout this work. The gas phase fugacity of solute i is

$$\hat{f}_i^V = \varphi_i p, \tag{A1}$$

where φ_i is the gas phase fugacity coefficient of solute i. Following the work of Maloney and Prausnitz,[34] the polymer phase fugacity of solute i is written as

$$\hat{f}_i^P = \Omega_i^* w_i H_i \exp\left(\int_0^p \frac{\overline{v}_i^{\infty} d\tilde{p}}{RT} \right), \tag{A2}$$

where w_i is the weight-fraction of solute i in the polymer phase (P), Ω_i^* is the weight-fraction activity coefficient, defined such that $\Omega_i^* \to 1$ as $w_i \to 0$, and H_i is the weight-average Henry's constant of solute i in the polymer. By defining K_i as $\Omega_i^* H_i \exp(\int_0^p \overline{v}_i^{\infty} d\overline{p}/RT)$, the polymer phase fugacity of solute i can be rewritten as

$$\hat{f}_i^P = K_i w_i . \tag{A3}$$

By equating the vapor and polymer phase fugacities of solute i, the following general expression for the weight-fraction of ethylene in the polymer phase is obtained as

$$w_i = \frac{\varphi_i p}{K_i}. \tag{A4}$$

At low pressures and low solubilities, $K_i \to H_i$, $\varphi_i \to 1$, and $w_i \to \mathrm{sol}_i$ (sol_i is the solubility of gas solute i in PE), leading to the Henry's law expression for gas i solubility in PE

$$\lim_{\substack{p \to 0 \\ w_i \to 0}} \mathrm{sol}_i = w_i = \frac{p}{H_i}. \tag{A5}$$

Note that in this form, Henry's constant H_i represents the proportionality factor between the solubility of solute i in the polymer and the pressure for low pressure conditions; H_i is often strongly dependent on temperature.

APPENDIX B: INFINITE DILUTION SIMULATIONS

One method to calculate the solubility of gas i in PE at infinite dilution is by using a test molecule insertion method.[9,17] In this method, an $N_{\mathrm{PE}}pT$ simulation is conducted and the infinite dilution chemical potential of gas i is calculated by a test-molecule insertion of solute i in the system by the same means as outlined in Sec. III D. In this method, the weight-average Henry's constant of solute i in PE can be shown to be given by

$$H_i = \left(\frac{MW_{\mathrm{PE}}}{MW_i} \right) \frac{\rho_{\mathrm{PE}}}{\beta} \exp(\beta \mu_i^{\mathrm{EX},\infty}), \tag{B1}$$

where ρ_{PE} is the pure polyethylene molar density at p and T. By making use of the same CB methods outlined in Sec. III B for the insertion of solute i in the pure polyethylene system, the excess chemical potential of i can be determined by

$$\beta \mu_i^{\mathrm{EX},\infty} = \ln\left(\frac{\langle V \rangle_{N_{\mathrm{PE}}pT}}{\langle V W_{\mathrm{test}\ i}^{\mathrm{ext}} \rangle_{N_{\mathrm{PE}}pT}} \right), \tag{B2}$$

where $W_{\mathrm{test}\,i}^{\mathrm{ext}}$ is the Rosenbluth weight for the test-particle insertion of solute i given by Eq. (8). Equation (B2) assumes that molecule i contains no intramolecular nonbonded interactions (i.e., only bond stretching, bond bending, and torsional interactions are present). This is the case for ethylene studied in this work. By inserting Eq. (B2) into (B1), the following is obtained for the weight-average Henry's constant of solute i in PE:

$$H_i = \left(\frac{MW_{\mathrm{PE}}}{MW_i} \right) \frac{\rho_{\mathrm{PE}}}{\beta} \frac{\langle V \rangle_{N_{\mathrm{PE}}pT}}{\langle V W_{\mathrm{test}\ i}^{\mathrm{ext}} \rangle_{N_{\mathrm{PE}}pT}}. \tag{B3}$$

Equation (B3) can be used with Eq. (A5) to evaluate the solubility as a function of pressure under the assumption of an ideal gas for the solute i.

APPENDIX C: THERMODYNAMIC RELATIONSHIPS FOR SOME PARTIAL MOLAR QUANTITIES

Recall the general thermodynamic relationships for pressure and temperature dependence of the fugacity of species i in a multicomponent mixture

$$\left(\frac{\partial \ln \hat{f}_i}{\partial p} \right)_{N_1, N_2, T} = \frac{\overline{v}_i}{RT}, \tag{C1}$$

$$\left(\frac{\partial \ln \hat{f}_i}{\partial T} \right)_{N_1, N_2, p} = -\frac{\overline{h}_i - h_i^{\dagger}}{RT^2}, \tag{C2}$$

where $h_i^{\dagger}$ is the enthalpy of pure component i in an ideal-gas state at the same temperature and pressure as the real mixture. Inserting Eq. (A3) into Eqs. (C1) and (C2), one obtains an expression for the effect of temperature and pressure on K_i as

$$\left(\frac{\partial \ln K_i(T,p)}{\partial p} \right)_{N_1, N_2, T} = \frac{\overline{v}_i}{RT}, \tag{C3}$$

$$\left(\frac{\partial \ln K_i(T,p)}{\partial T} \right)_{N_1 N_2, p} = -\frac{\overline{h}_i - h_i^{\dagger}}{RT^2}. \tag{C4}$$

At a given condition, $\overline{v}_i$ can be calculated by the method outlined in Sec. IV. With $\overline{v}_i$ known, K_i can be extrapolated for various pressures by integrating Eq. (C3) from a given reference condition

$$K_i(T,p) = K_i^0(T,p^0)\exp\left(\int_{p^0}^{p} \frac{\overline{v_i}}{RT} d\overline{p} \right), \tag{C5}$$

where the superscript 0 is the reference condition. Assuming $\overline{v_i}$ is independent of pressure at a given temperature (satisfactory for moderate changes), Eq. (C5) can be further reduced into a simpler expression for K_i as

$$K_i(T,p) = K_i^0(T,p^0)\exp\left(\frac{\overline{v_i^0}(p-p^0)}{RT} \right). \tag{C6}$$

[1] S. K. Nath and J. J. de Pablo, J. Phys. Chem. B **103**, 3539 (1999).
[2] S. K. Nath, B. J. Banaszak, and J. J. de Pablo, Macromolecules **34**, 7841 (2001).
[3] U. H. E. Hansmann, Chem. Phys. Lett. **281**, 140 (1997).
[4] Q. Yan and J. J. de Pablo, J. Chem. Phys. **111**, 9509 (1999).
[5] A. Z. Panagiotopoulos, Mol. Phys. **61**, 813 (1987).
[6] A. Z. Panagiotopoulos, N. Quirke, M. Stapleton, and D. J. Tildesley, Mol. Phys. **63**, 527 (1988).
[7] A. Z. Panagiotopoulos, Int. J. Thermophys. **10**, 447 (1989).
[8] A. Z. Panagiotopoulos, Mol. Simul. **9**, 1 (1992).
[9] D. Frenkel and B. Smit, *Understanding Molecular Simulation: From Algorithms to Applications* (Academic, New York, 1996), pp. 31–33, 113–123, 157–163, 291–300, 316–332, 410.
[10] T. Spyriouni, I. G. Economou, and D. N. Theodorou, Phys. Rev. Lett. **80**, 4466 (1998).
[11] S. K. Nath, F. A. Escobedo, and J. J. de Pablo, J. Chem. Phys. **108**, 9905 (1998).
[12] S. K. Nath, B. J. Banaszak, and J. J. de Pablo, J. Chem. Phys. **114**, 3612 (2001).
[13] S. K. Nath and J. J. de Pablo, Mol. Phys. **98**, 231 (2000).
[14] W. L. Jorgensen, J. D. Madura, and C. J. Swensen, J. Am. Chem. Soc. **106**, 6638 (1984).
[15] S. K. Nath, F. A. Escobedo, J. J. de Pablo, and I. Patramai, Ind. Eng. Chem. Res. **37**, 3197 (1998).
[16] M. P. Allen and D. J. Tildesley, *Computer Simulation of Liquids* (Oxford University Press, New York, 1987), pp. 64–65.
[17] J. J. de Pablo, M. Laso, and U. W. Suter, Macromolecules **26**, 6180 (1993).
[18] M. N. Rosenbluth and A. W. Rosenbluth, J. Chem. Phys. **23**, 356 (1955).
[19] S. Duane, A. D. Kennedy, B. J. Pendleton, and D. Roweth, Phys. Lett. B **195**, 216 (1987).
[20] S. K. Nath, J. J. de Pablo, and A. D. DeBellis, J. Am. Chem. Soc. **121**, 4252 (1999).
[21] R. Faller and J. J. de Pablo, J. Chem. Phys. **116**, 55 (2002).
[22] R. Faller and J. J. de Pablo, J. Chem. Phys. **119**, 7605 (2003).
[23] H. J. C. Berendsen, J. P. M. Postma, W. F. Gunsteren, A. DiNola, and J. R. Haak, J. Chem. Phys. **81**, 3684 (1984).
[24] W. F. Gunsteren and H. J. C. Berendsen, Angew. Chem., Int. Ed. Engl. **29**, 992 (1990).
[25] M. Laso, J. J. de Pablo, and U. W. Suter, J. Chem. Phys. **97**, 2817 (1992).
[26] F. A. Escobedo and J. J. de Pablo, J. Chem. Phys. **105**, 4391 (1996).
[27] J. I. Siepmann and D. Frenkel, Mol. Phys. **75**, 59 (1992).
[28] B. Smit and J. I. Siepmann, J. Phys. Chem. **98**, 8442 (1994).
[29] G. Marsaglia, Ann. Math. Stat. **43**, 645 (1972).
[30] Z. Chen and F. A. Escobedo, J. Chem. Phys. **113**, 11382 (2000).
[31] Q. Yan and J. J. de Pablo, J. Chem. Phys. **113**, 1276 (2000).
[32] R. L. Cotterman and J. M. Prausnitz, AIChE J. **32**, 1799 (1986).
[33] G. T. Dee, T. Ougizawa, and D. J. Walsh, Polymer **33**, 3462 (1992).
[34] D. P. Maloney and J. M. Prausnitz, AIChE J. **22**, 74 (1976).